

Subject-specific biomechanics of trunk: musculoskeletal scaling, internal loads and intradiscal pressure estimation

F. Ghezelbash¹ · A. Shirazi-Adl¹ · N. Arjmand² · Z. El-Ouaaid^{1,3} · A. Plamondon³

Received: 20 November 2015 / Accepted: 25 April 2016 / Published online: 12 May 2016
© Springer-Verlag Berlin Heidelberg 2016

Abstract Development of a subject-specific computational musculoskeletal trunk model (accounting for age, sex, body weight and body height), estimation of muscle forces and internal loads as well as subsequent validation by comparison with measured intradiscal pressure in various lifting tasks are novel, important and challenging. The objective of the present study is twofold. First, it aims to update and personalize the passive and active structures in an existing musculoskeletal kinematics-driven finite element model. The scaling scheme used an existing imaging database and biomechanical principles to adjust muscle geometries/cross-sectional-areas and passive joint geometry/properties in accordance with subjects' sex, age, body weight and body height. Second, using predictions of a detailed passive finite element model of the ligamentous lumbar spine, a novel nonlinear regression equation was proposed that relates the intradiscal pressure (IDP) at the L4–L5 disc to its compression force and intersegmental flexion rotation. Predicted IDPs and muscle activities of the personalized models under various tasks are found in good-to-excellent agreement with reported measurements. Results indicate the importance of

personal parameters when computing muscle forces and spinal loads especially at larger trunk flexion angles as minor changes in individual parameters yielded up to 30 % differences in spinal forces. For more accurate subject-specific estimation of spinal loads and muscle activities, such a comprehensive trunk model should be used that accounts for subject's personalized features on active musculature and passive spinal structure.

Keywords Musculoskeletal model · Trunk biomechanics · Finite element · Subject specific · Intradiscal pressure · Spinal loads

1 Introduction

The role of biomechanical factors in low back pain (da Costa and Vieira 2010; Ferguson and Marras 1997; Heneweer et al. 2011) and disc degeneration (Adams and Roughley 2006) has long been realized. Due to the invasive nature of in vivo attempts to estimate spinal loads via intradiscal pressure sensors (Nachemson 1960; Sato et al. 1999; Schultz et al. 1982; Wilke et al. 1999) and instrumented vertebral implants (Dreischarf 2015; Rohlmann et al. 2013), musculoskeletal biomechanical models have emerged as a essential, robust and accurate alternative and complementary tools (Reeves and Cholewicki 2003).

In comparison with the existing optimization-driven (Christophy et al. 2012; De Zee et al. 2007; Khurelbaatar et al. 2015), EMG-driven (Granata and Marras 1995; Jia et al. 2011; van Dieën et al. 2003) and hybrid (Cholewicki and McGill 1996; Gagnon et al. 2011; Mohammadi et al. 2015) trunk models, our kinematics-driven (KD) nonlinear finite element (FE) musculoskeletal model of the trunk has demonstrated its validity and predictive power in a broad

✉ A. Shirazi-Adl
aboulfazl.shirazi@polymtl.ca

¹ Division of Applied Mechanics, Department of Mechanical Engineering, Ecole Polytechnique, Montréal, Québec, Canada

² Department of Mechanical Engineering, Sharif University of Technology, Tehran, Iran

³ Institut de recherche Robert Sauvé en santé et en sécurité du travail, Montréal, Québec, Canada

range of applications from static (Arjmand and Shirazi-Adl 2006a; El-Rich et al. 2004) to dynamic (Bazrgari et al. 2008; Shahvarpour et al. 2015b) and stability analyses (Bazrgari and Shirazi-Adl 2007; Ouaid et al. 2009; Shahvarpour et al. 2015a). It takes account of nonlinear passive properties of both ligamentous spine and muscles, muscle wrapping (Arjmand et al. 2006), all translational degrees of freedom (Ghezelbash et al. 2015; Meng et al. 2015), physiological partitioning of gravity, inertia and damping at different segments and satisfaction of equilibrium conditions at all lumbar/thoracolumbar joints and directions (Arjmand et al. 2007). Moreover, it considers the stiffening role of compressive forces on passive responses of motion segments (Gardner-Morse and Stokes 2004; Shirazi-Adl 2006).

Due to anthropometric differences between individuals, personalization or scaling schemes have been introduced in some model studies. For instance, imaging techniques have been used to reconstruct individual muscles geometry and bony structures (Gerus 2013; Martelli et al. 2015; Valente et al. 2015). This approach, though accurate, is however time-consuming, expensive and semi-automated. Alternatively, scaling factors (isotropic or anisotropic) have been employed for model adaptation (Damsgaard et al. 2006; Delp 2007; Rasmussen et al. 2005). Though being fast and automated, the method is heuristic with simplifications that can cause errors (Scheys et al. 2008). Using AnyBody Modelling System (AMS) and the scaling technique, effect of changes in body weight (BW: 50–120 kg) and body height (BH: 150–200 cm) on spinal loads was investigated (Han et al. 2013). Although spinal loads altered nearly linearly with changes in both BW and BH but the effect of the former on response was found to be much greater than that of the latter. In this model study, linear scaling was used in the model geometry and muscle cross-sectional areas. The corresponding effects of personal factors on spinal passive properties were not simulated. Recently, an optimization-based scaling method for dynamic tasks that require motion capture measurements have been proposed (Lund et al. 2015). Hajhosseinali et al. (2015) developed an automated anisotropic scaling method where the geometry (area and lever arm) of each muscle was altered in accordance with imaging data sets (Anderson et al. 2012) while accounting for variations only in the subject's BW. It is evident, hence, that a comprehensive, automated and accurate image-based method has not yet been introduced to personalize models. Moreover, existing scaling methods overlook expected crucial alterations in spinal passive properties as well as moment arms of muscles and gravity load at different levels as age, sex, BW and BH change.

Moreover and due to the importance of validation of model predictions and existence of in vivo data on the intradiscal pressure (IDP) during various activities (Nachemson 1960; Sato et al. 1999; Wilke et al. 2001), it is important to compare estimated spinal compression forces to the corresponding

IDP values measured in vivo. Shirazi-Adl and Drouin (1988) reported the effect of the axial compression when combined with some flexion moment on IDP at the L2–L3 level, while Dreischarf et al. (2013) proposed a correction factor when estimating IDP from the compression force and L4–L5 disc area. Despite earlier attempts and based on results of a validated lumbar spine model under single and combined sagittal plane loading (Shirazi-Adl 2006), it is crucial to develop a comprehensive nonlinear regression equation relating the L4–L5 IDP not only to the compression force but the sagittal rotation as well.

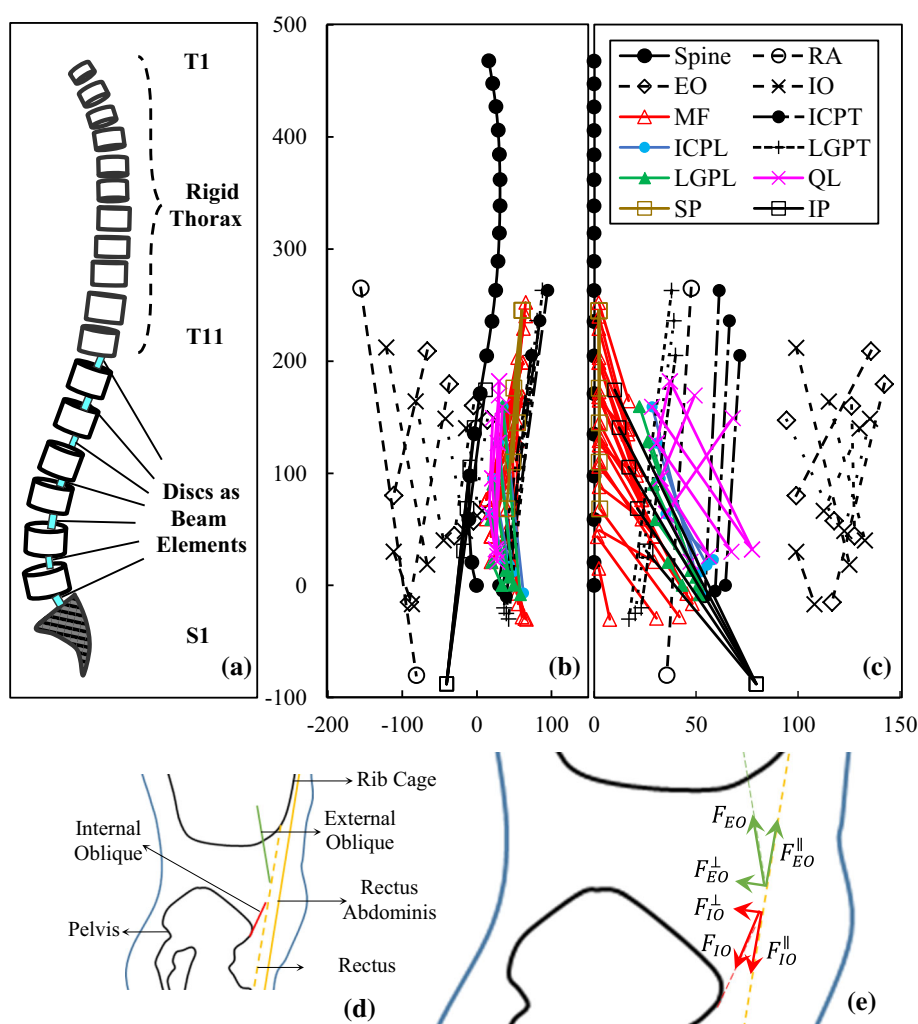
The objectives of this study are, therefore, set to update and personalize, apply and validate the existing iterative nonlinear KD–FE model as well as to develop a nonlinear regression equation for compression force-sagittal rotation-IDP relation. For the former, following improvements are made: 1. The muscle architecture is extended, 2. A new technique of modelling rectus sheath and abdominal muscles is developed, 3. An additional deformable intervertebral disc (T11–T12) is added, and 4. A generic method to personalize the model based on BW, BH, age and sex is introduced. The presented method accounts for changes in both muscle geometries (length, area and lever arm) and passive properties of joints. A nonlinear regression equation is subsequently developed to estimate IDP as a function of the compression and the sagittal intersegmental angle. Estimated compression and muscle forces are validated by comparison with available in vivo measurements (Arjmand et al. 2010; Ouaid et al. 2013; Wilke et al. 2001).

2 Methods

2.1 Finite element model

A sagittally symmetric FE model of the spine (T1–S1), representing bony structures and soft tissues, is reconstructed in Abaqus (Simulia Inc., Providence, RI, USA). Original nodal coordinates are used for the spinal geometry (Fig. 1) (Kiefer et al. 1998; Shirazi-Adl et al. 2005). Nonlinear passive responses of seven lower motion segments (including vertebrae, discs, facets and ligaments) are modelled by Timoshenko beam elements with quadratic displacement fields. In addition to T12–S1 motion segments with nonlinear passive properties (moment-curvature and force-strain) at three physiological planes (Fig. 2) (Bazrgari 2008; Shirazi-Adl 1994a, 2006), the T11–T12 motion segment is also added with passive properties based on those of the T12–L1 motion segment (Oxland et al. 1992) modulated according to their respective disc area and height using conventional beam theory. Furthermore, bending properties of the T11–T12 motion segment are subsequently increased by 20% to account for the rib cage stiffness (Brasiliense et al. 2011; Watkins 2005).

Fig. 1 A schematic depiction of the **a** finite element model, **b** muscle architecture in the sagittal plane, **c** muscle architecture in the frontal plane, **d** rectus sheath anatomy in the sagittal plane, and **e** rectus sheath load interaction in the sagittal plane. *ICPL* iliocostalis pars lumborum, *ICPT* iliocostalis pars thoracic, *IP* iliopsoas, *LGPL* longissimus pars lumborum, *LGPT* longissimus pars thoracic, *MF* multifidus, *QL* quadratus lumborum, *IO* internal oblique, *EO* external oblique, *RA* rectus abdominis, F_{EO} force in the EO upper most fascicle, F_{EO}^{\parallel} the projection of F_{EO} onto the rectus sheath, F_{EO}^{\perp} the projection of F_{EO} onto the direction normal to the rectus sheath, F_{IO} force in the IO lowermost fascicle, F_{IO}^{\parallel} the projection of F_{IO} onto the rectus sheath, F_{IO}^{\perp} the projection of F_{IO} onto the direction normal to the rectus sheath



Deformable beam elements are shifted 4 mm posteriorly to partially account for changes in the centre of rotation under loads (Shirazi-Adl et al. 1986). Vertebrae and remaining T1–T11 motion segments are modelled by rigid elements. Trunk weight is distributed eccentrically and applied via rigid links to corresponding vertebrae (Pearsall 1994); additionally, weights of upper arms, lower arms and head are applied at their centres of mass (De Leva 1996).

2.2 Muscle architecture and wrapping

The existing muscle architecture (Arjmand and Shirazi-Adl 2006b; El-Rich et al. 2004; Shirazi-Adl et al. 2005) is revised for the current study. New global fascicles of the longissimus and iliocostalis are added due to the addition of the T11–T12 motion segment (Stokes and Gardner-Morse 1999). Muscle architecture of the quadratus lumborum and multifidus is refined by the addition of local and inter-segmental fascicles (Phillips et al. 2008; Stokes and Gardner-Morse 1999). The intersegmental spinalis muscle is also introduced

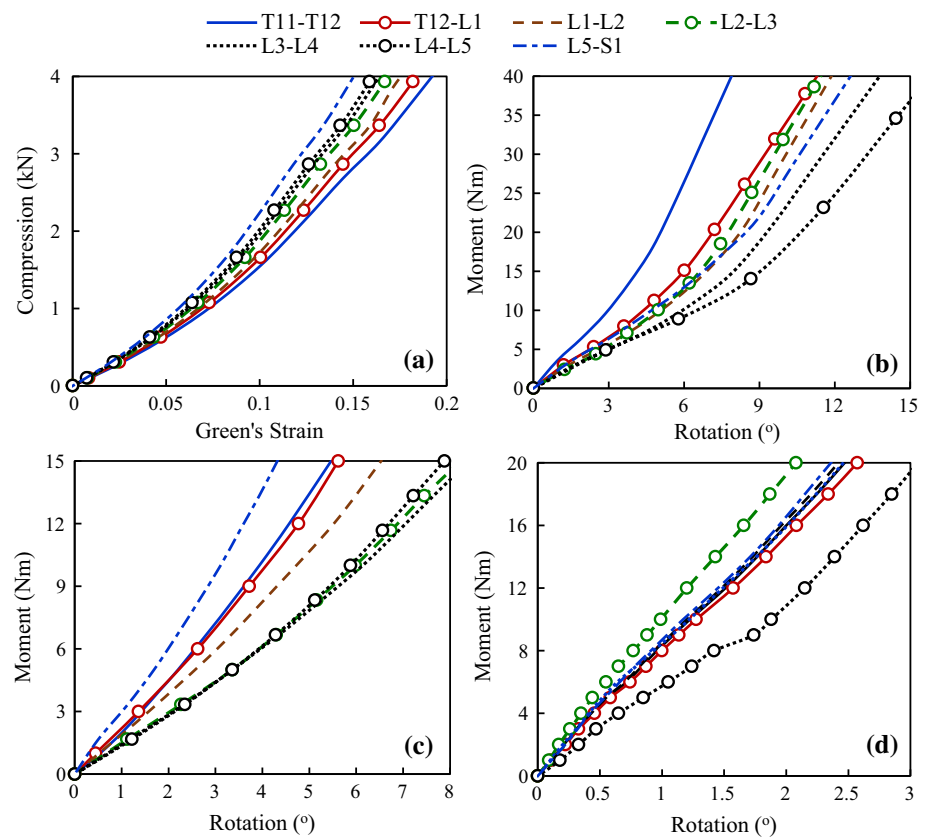
(Delp et al. 2001; Gilroy 2008). Furthermore, the geometry of abdominal muscles (rectus abdominis, internal oblique and external oblique) is updated (Stokes and Gardner-Morse 1999) accounting for the geometry of the rib cage (Gayzik et al. 2008). The new sagittally symmetric muscle architecture includes 126 muscles (Fig. 1).

Muscles as deformable bodies develop contact forces with surrounding tissues and change line of action when wrap around vertebrae during trunk movements. This wrapping contact phenomenon is simulated by an algorithm which accounts both for the curved paths of the global extensor muscles as well as their contact forces (Arjmand et al. 2006).

2.3 Rectus sheath

Some fascicles of the internal and external obliques are attached to the semilunar line (Brown et al. 2011; McGill 1996). According to the muscle architecture, the uppermost fascicles of the external oblique and the lowermost fascicles of the internal oblique are inserted into the rectus

Fig. 2 Passive property curves in **a** axial force (Shirazi-Adl 2006), **b** flexion moment (Shirazi-Adl 2006), **c** lateral moment (Shirazi-Adl 1994a), and **d** torsion (Shirazi-Adl 2006)



sheaths (see Fig. 1). The rectus sheaths, modelled separately on the left and the right side of RA, transfer tensile forces of muscle fascicles attached to them directly to the rib cage and pelvic bone. Forces of corresponding fascicles (F_{EO} and F_{IO} , Fig. 1) are projected onto the rectus sheaths (F_{EO}^{\parallel} and F_{IO}^{\parallel} , Fig. 1), while remaining components (F_{EO}^{\perp} and F_{IO}^{\perp} , Fig. 1) on both sides of rectus abdominis partially cancel each other in symmetric lifts or are assumed in general (symmetric and asymmetric lifts) to be counterbalanced by forces in transverse abdominal muscle (neglected in the current model) and intra-abdominal pressure (IAP). Besides, the upper rectus sheaths can transfer tension only; the projected force of the internal oblique minus that of the external oblique on the rectus sheath must be positive on each side pulling the rib cage downward ($F_{IO}^{\parallel} - F_{EO}^{\parallel} \geq 0$).

2.4 Muscle force calculation

For each iteration, known measured segmental and pelvic rotations (or equivalently angular velocities in dynamic simulations), ω_i where $i \in \mathcal{J} := \{T11, \dots, S1\}$, are iteratively prescribed into the FE model and associated required moments are used as equality equilibrium equations when estimating muscle forces (Eq. 1, see also the flowchart in

Fig. 3). Due to redundancy, an optimization algorithm with the cost function of quadratic sum of muscle stresses is used (Arjmand and Shirazi-Adl 2006c) with equilibrium equations applied as equality constraints:

$$\sum_i (r_i^j - o^j) \times f_i^j = m^j, \quad (1)$$

where $j \in \mathcal{J}$; f_i^j is the force vector of a muscle fascicle which is attached to the j th vertebra. r_i^j and o^j are position vectors of the corresponding muscle force and j th vertebra, respectively. Also, m^j is the required moment at j th level evaluated iteratively by the nonlinear FE model. Besides, muscle forces are constrained to be positive and greater than their passive forces (Davis et al. 2003) and smaller than the sum of maximum active forces, $0.6 \text{ MPa} \times \text{physiological cross-sectional area (PCSA)}$ (Winter 2009), plus the passive forces. In more demanding activities simulated in this study such as tasks 3, 8 and 10–12 (Table 1), the maximum stress of 0.6 MPa was increased to 1.0 MPa to avoid excessive constraint on some muscle forces.

For the subsequent iterations, the updated muscle forces are applied onto their vertebrae as additional penalty forces and the analysis is repeated till convergence reached (no or $< 1\%$ changes in muscle forces between two successive iterations).

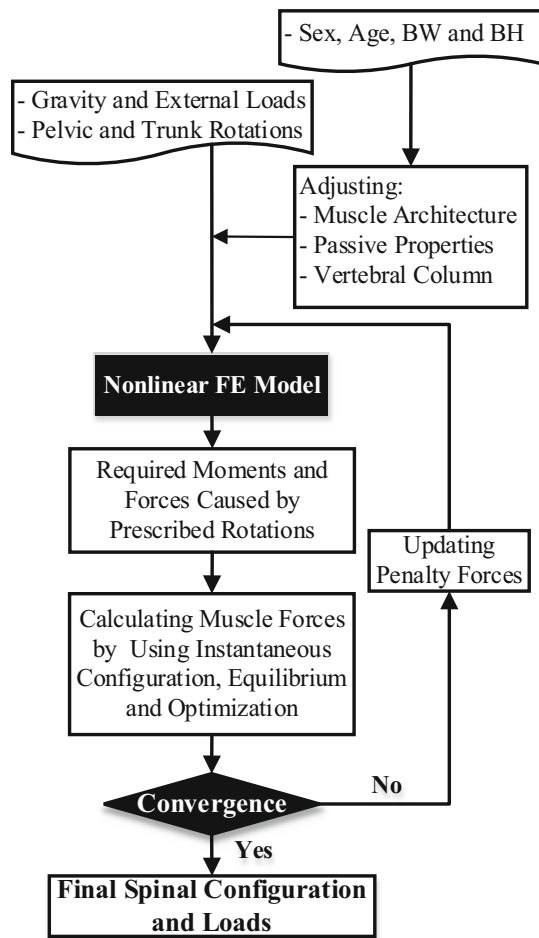


Fig. 3 The flowchart of the kinematics-driven, nonlinear FE musculoskeletal model

2.5 Simulated tasks

The performance of the model is investigated in a number of tasks and estimated spinal loads and muscle activities are compared with corresponding measured IDPs and EMG data when available. IDPs in relaxed upright standing, flexed postures, asymmetric lifting and lateral bending are compared with in vivo measurements (Wilke et al. 2001). Furthermore, measured EMG activities (Arjmand et al. 2010; Ouaaid et al. 2013) are compared with estimated muscle activities during forward flexion and maximum voluntary exertions (MVEs) in flexion, extension and twisting (see Table 1).

2.6 Prescribed rotations

To initially establish the upright standing posture under gravity alone as the reference condition in all tasks, prescribed rotations from the initial undeformed configuration are obtained from the following optimization problem (Shirazi-Adl et al. 2002):

Table 1 Description of all simulated tasks

No.	Description
1	Standing relaxed posture with no load in hands
2	Standing posture while holding a 19.8 kg close to the body (Arjmand et al. 2011; Wilke et al. 2001)
3	Standing posture while holding a 19.8 kg away from the body (Arjmand et al. 2011; Wilke et al. 2001)
4	Trunk flexion at 50° with no load in hands (Arjmand et al. 2011; Wilke et al. 2001)
5	Full trunk flexion (107.3°) with no load in hands (Arjmand et al. 2011; Wilke et al. 2001)
6	Trunk flexion at 70° with 19.8 kg load in hands (Arjmand et al. 2011; Wilke et al. 2001)
7	Forward flexion from the upright posture at 10° intervals (Arjmand et al. 2009, 2010)
8	One-handed asymmetric lifting of 19.8 kg load (Rajaei et al. 2015)
9	Trunk lateral bendings at 10° and 20° with no load in hands (Wilke et al. 2001)
10	Maximum voluntary exertion (MVE) in extension under 242 Nm ^a extension moment (Ouaaid et al. 2013)
11	Maximum voluntary exertion (MVE) in flexion under 151 Nm ^a flexion moment (Ouaaid et al. 2013)
12	Maximum voluntary exertion (MVE) in torsion under 78.3 Nm right axial torque with 21.1 right lateral and 16.7 flexion moments (Arjmand et al. 2008)

^a Mean measured moments of 12 subjects (Ouaaid et al. 2013)

$$\min_{\Omega} \sum_{i \in \mathcal{J}} |m^i(\Omega)| \quad (2)$$

where \mathbf{m} is the required moment vector and $\Omega := \{\omega_{\alpha} | \alpha \in \mathcal{J}\}$. The initial guess, Ω_0 , is made manually, and upper and lower bounds of the optimization problem are assumed to be $\pm 5^\circ$ of Ω_0 . The forgoing optimization problem is solved for each subject after the scaling (see the following section for scaling). In task 8, the trunk is rotated 5° towards flexion in accordance with (Wilke et al. 2001), and in task 3, the following rotations are prescribed onto the undeformed initial posture (El-Rich and Shirazi-Adl 2005) in accordance with (Wilke et al. 2001): -2.0° at T11, 4.0° at T12, 10.9° at L1, 15.8° , at L2, 14.5° at L3, 9.9° at L4, 4.9° at L5, and 4.9° at S1 where positive values are extension.

In flexion (tasks 4–7 in Table 1), the lumbopelvic rhythm is taken from in vivo measurements (Arjmand et al. 2009, 2010). The total T11–S1 rotation is then partitioned among T11–L5 vertebrae with 6.0% for T11–T12, 10.9% for T12–L1, 14.1% for L1–L2, 13.2% for L2–L3, 16.9% for L3–L4, 20.1% for L4–L5, and 18.7% for L5–S1 (Arjmand et al.

2009, 2010; Gercek et al. 2008; Hajibozorgi and Arjmand 2016).

In lateral bending tasks (task 9 in Table 1), rotation proportions for the T11–T12 down to the L5–S1 levels are set to be 8.3, 2.8, 9.4, 18.3, 22.8, 25.6 and 12.8%, respectively (Gercek et al. 2008; Rozumalski et al. 2008; Shirazi-Adl 1994a). In accordance with (Paterson and Burn 2012), the sacral lateral rotation varies linearly from 0° to 2° as the trunk lateral rotation reaches 20° of lateral bending.

For extension and flexion MVE tasks, rotations of 9° and –13° at the T11 and 16° and 13° at the S1 (positive: extension) are considered, respectively. These rotations are subsequently partitioned between the vertebrae (T11–S1) in accordance with aforementioned flexion rotation proportions. It is to be noted that the earlier proposed rotations (Ouaaid et al. 2013) were altered slightly when simulating semi-seated posture in the current model.

2.7 Model scaling

Model scaling (personalization) is required since subjects with different individual parameters, i.e., sex, age, BH and BW, participated in various experimental studies (Arjmand et al. 2009, 2010; Ouaaid et al. 2013; Wilke et al. 2001). Biomechanical principles in conjunction with regression equations derived from medical imaging databases (Anderson et al. 2012; Shi et al. 2014), are employed. Inputs of regression equations are the subject's personal parameters (sex, age, BW and BH). To find the reference personal parameters that best match with the reported regression equations (Anderson et al. 2012), a least absolute deviation (LAD) problem is initially solved:

$$\min_F \left[\sum_{i \in \mathcal{M}} \left(\left| i\overline{AP}^{\text{Model}} - i\overline{AP}^{\text{Reg}}(F) \right| + \left| i\overline{ML}^{\text{Model}} - i\overline{ML}^{\text{Reg}}(F) \right| \right) \right], \quad (3)$$

where F is the personal parameter vector, $F = [\text{sex, age, BH, BW}]$; \mathcal{M} is the set containing all muscle groups, $\mathcal{M} := \{\text{rectus abdominis, external oblique, } \dots, \text{longissimus}\}$. $i\overline{AP}$ and $i\overline{ML}$ denote average anterior–posterior and medio-lateral distances of i th muscle ($i \in \mathcal{M}$) from vertebrae. Model and Reg superscripts represent distances calculated in the reference model from the muscle architecture (Fig. 2), and distances obtained from regression equations (Anderson et al. 2012), respectively. Results of the optimization process is sensitive to the lower bound of BH. Hence, 173 cm is assigned as the lower bound of BH because it is not rational that spine length to BH becomes larger than 0.27 (estimated based on Keller et al. (2005)).

Afterwards, coordinates of the vertebrae, discs, head and arms alter proportionally with changes in BH (e.g., $(x, y, z)_{\text{spine}} \propto \text{BH}/\text{BH}_{\text{Ref}}$, where BH_{Ref} is obtained from Eq. 3). For the muscle architecture, z -coordinates (cranial-caudal) remain proportional to BH (e.g., $z_{\text{RectusAbdominis}} \propto \text{BH}/\text{BH}_{\text{Ref}}$). To adjust anterior–posterior and medio-lateral distances as well as PCSAs, the regression equations (Anderson et al. 2012) are first normalized to their reference counterparts (calculated from the reference personal parameters). Then, for the subject-specific model, the average anterior–posterior distances from vertebrae normalized to the reference values (Fig. 1) are adapted according to the normalized regression equations. Similar process is performed for medio-lateral distances and PCSAs.

Furthermore, we utilize the conventional beam theory to alter passive joint properties (compression force-strain and moment-curvature relations). Three beam (or disc) parameters are used: 1- height, 2- area and 3- area moments. The disc height is assumed to be commensurate with BH (disc height $\propto \text{BH}/\text{BH}_{\text{Ref}}$) (Han et al. 2013), and the disc area is changed in accordance with A/A_{Ref} , in which A is the maximum cross-sectional area of the rib cage in the transverse plane for a given set of personal parameters (Shi et al. 2014); and A_{Ref} is the maximum cross-sectional area of the rib cage in the transverse plane for the reference personal parameters (disc area $\propto A/A_{\text{Ref}}$) (Shi et al. 2014). Additionally, area moments are assumed to be proportional to the disc area squared (area moments $\propto (A/A_{\text{Ref}})^2$).

2.8 Intra-abdominal pressure

Intra-abdominal pressure (IAP) is simulated in MVE tasks with concurrent activity in abdominal muscles. IAP is modelled as a follower load normal to the diaphragm reaching 10 and 25 kPa (Ouaaid et al. 2013), while the diaphragm area is modified based on (Shi et al. 2014). The resultant force is transmitted to the T11 via a rigid link with an anterior lever arm of 5 cm (Arjmand and Shirazi-Adl 2006b).

2.9 External loads

In tasks 1–7 (Table 1), positions of upper arms, lower arms, head and the external load in hands are based on measurements. For asymmetric lifting (task 8), the external load is taken at 34 cm lateral and 0 cm anterior–posterior to the L5–S1 disc (Rajaei et al. 2015). A concentrated force applied at the T8 (task 10) or T6 (task 11) simulates MVE in extension or flexion, respectively (Ouaaid et al. 2013). In the task 12 (Table 1), 78.3 Nm right axial torque with 21.1 right lateral and 16.7 flexion coupled moments are simultaneously applied at the T9 (Arjmand et al. 2008; Ng et al. 2001, 2002).

2.10 IDP estimation

A novel nonlinear regression equation for estimating IDP in the model is developed in this study. Inputs of this model are the compressive force (applied by a wrapping element) and the intersegmental rotation (under various sagittal moments) at the L4–L5 disc taken based on unpublished results (4 compressions levels at 16 intersegmental rotations each) of a validated lumbar spine FE model (Shirazi-Adl 1994a, b; Shirazi-Adl and Pamianpour 1993). The quadratic regression equation is developed relating model output (i.e., IDP) to its inputs being compression force and sagittal rotation at the L4–L5 level.

2.11 Additional constraints

A set of constraints is introduced for task 11 (see Table 1) to reduce excessively large required flexion moments at lumbar levels (Bazrgari et al. 2009; Ouaid et al. 2013):

$$\sum f_i^{T11} \cdot t_{AP}^{T11} = F_S^{T11}, \tag{4a}$$

$$\left[\sum f_i^{T11} + \sum f_i^{T12} \right] \cdot t_{AP}^{T12} = F_S^{T12}, \tag{4b}$$

where f_i^{T11} and f_i^{T12} denote muscle force vectors at the T11 and T12. t_{AP}^{T11} and t_{AP}^{T12} are unit vectors pointing towards anterior–posterior shear direction at the centre of T11 and T12. F_S^{T11} and F_S^{T12} represent required shear forces at the T11 and T12 levels to diminish flexion moments at local lumbar levels (Bazrgari et al. 2009); minimal values of F_S^{T11} and F_S^{T12} are found iteratively. In addition and based on recorded EMG at antagonist muscles (Ouaid et al. 2013), coactivation of antagonist muscles at flexion and extension MVE tasks are generated via additional constraints:

$$\sum_{a \in \mathcal{A}} (r_a^{T11} - o^{T11}) \times f_a^{T11} = m_A, \tag{5}$$

where \mathcal{A} is the set including antagonist muscles attached to the T11, and m_A is the assumed antagonist moment generated antagonist muscles. It is to be noted that due to the symmetry in flexion and extension MVE tasks, only sagittal component of Eq. 5 is considered in this study.

3 Results

3.1 IDP regression equation

Regression analysis using unpublished results of the detailed FE model of the lumbar spine (Shirazi-Adl 2006) for the L4–L5 motion segment yields the following quadratic equation:

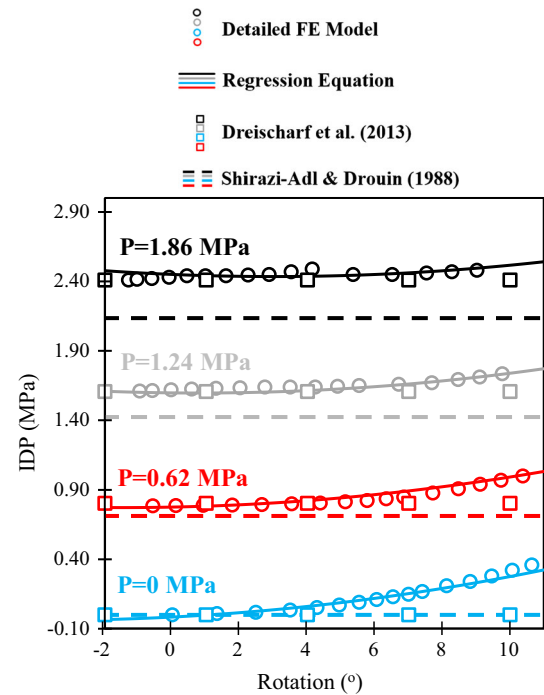


Fig. 4 Estimated intradiscal pressures (IDPs) at the L4–L5 from the detailed FE model (Shirazi-Adl 2006), regression equation (Eq. 6), proposed relation of (Dreischarf et al. 2013) ($IDP = P/0.77$), and proposed curve of (Shirazi-Adl and Drouin 1988) (at the L2–L3) under pure axial force with the following colour code: blue (bottom) $P = 0$ MPa; red $P = 0.62$ MPa; grey $P = 1.24$ MPa; black (top) $P = 1.86$ MPa, where P is the nominal pressure (compression/disc area) with the disc area of 1455 mm^2

$$IDP(P, \theta) = -1.556 \times 10^{-2} + 1.255P + 1.243 \times 10^{-2}\theta + 3.988 \times 10^{-2}P^2 - 1.212 \times 10^{-2}P\theta + 1.669 \times 10^{-3}\theta^2, \tag{6}$$

where P (MPa) is the nominal pressure (compression/total disc cross-sectional area) and θ ($^\circ$, positive in flexion) is the intersegmental flexion rotation. The coefficient of determination, R^2 , and root mean squared error (RMSE) of the regression equation are, respectively, 0.999 and 0.025 MPa showing the goodness of fit. It is noteworthy that we derived the appropriate set of data (P, θ) from (compression, θ) by considering the disc area of 1455 mm^2 (Shirazi-Adl 1994a). Results of the detailed FE model (Shirazi-Adl 2006), Eq. 6, Shirazi-Adl and Drouin (1988) under pure compression, and Dreischarf et al. (2013) show differences that grow with the applied compression and segmental rotation (Fig. 4). Hereafter, Eq. 6 is employed for IDP estimations.

3.2 Upright neutral standing posture

Solving the optimization of required moments (Eq. 2) to set the upright neutral standing posture under gravity for four different personal parameters that are used in this study leads to

Table 2 Computed rotations (from undeformed geometry to construct the spinal configuration under gravity in the upright standing, positive values: extension) from the optimization of moments (Eq. 3) for 4 different personal parameters used in this study

Personal parameters				
Sex	Male	Male	Male	Male
Age	30	25	45	52
BH	1.80	1.78	1.74	1.75
BW	73	73	72	68
Rotations (°)				
T11	-7.52	-7.69	-7.68	-7.65
T12	-4.71	-4.70	-4.79	-4.80
L1	-0.93	-0.80	-1.09	-1.16
L2	2.55	2.29	2.49	2.42
L3	5.01	5.12	5.21	5.10
L4	6.77	6.80	6.78	6.90
L5	8.04	8.00	8.09	8.22
S1	9.59	10.04	9.65	9.70

sagittal rotations (from the initial unloaded geometry) presented in Table 2 using the reference personal parameters (Eq. 3) as sex = male, age = 41.8 year, BH = 173.0 cm, and BW = 75.1 kg.

3.3 Validation

For the simulated tasks, the correlation coefficient and RMSE between measured (Wilke et al. 2001) and estimated IDPs (Fig. 5) are 0.984 and 0.14 MPa, respectively, demon-

strating satisfactory IDP predictions both pattern-wise and magnitude-wise. In forward flexion (task 7), estimated activities of global longissimus and iliocostalis muscles follow trends similar to the measured EMG signals (Arjmand et al. 2010) (Fig. 6a) and showing flexion relaxation phenomenon. The substantial drop in active force components accompany reverse trends in passive forces of these global extensor muscles as trunk flexion reaches its peak of 107° (Fig. 6b). At this full flexion, curved trajectory and large wrapping forces at different levels are computed in both global extensor muscles (Fig. 6c).

Good agreement is also found in MVE tasks in extension under 242 Nm (Fig. 7a) and in flexion under 151 Nm (Fig. 7b) when comparing estimations of the model (personalized based on averaged parameters of all 12 subjects) versus mean of recorded EMG in 12 male subjects (with the average age, BW and BH of 25 years, 72.98 kg and 177.67 cm) for superficial back and abdominal muscles (Ouaaid et al. 2013). Applied IAPs, antagonistic coactivation moments (Eq. 5) and shear forces (Eq. 4) as well as correlation coefficients between estimated and measured muscle activities for MVE tasks are listed in Table 3. Additionally and under the reference upright posture, good agreements are noted in estimated muscle activities versus measured ones (Ng et al. 2001) on right (Fig. 8a) and left (Fig. 8b) sides for MVE in torsion.

3.4 Effects of personal parameters

The effect of changes in personalized parameters of subjects in earlier works (Arjmand et al. 2010; Ouaaid et al. 2013;

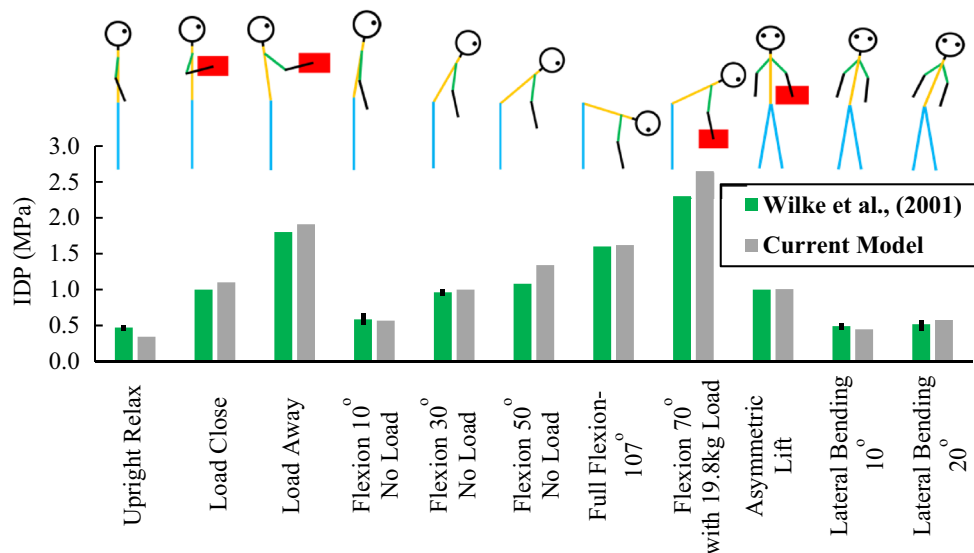


Fig. 5 Measured intradiscal pressure (IDP) (Wilke et al. 2001) versus calculated IDPs of the model at the L4–L5 level; the model is personalized here to match the personal parameters of the subject participated

in the in vivo study of Wilke et al. (2001): sex = male, age = 45 years, BW = 72 kg and BH = 173.9 cm

Fig. 6 a Comparison between estimated activities (i.e., force divided by 0.6MPa times PCSA) of right and left longissimus pars thoracic (LGPT) and iliocostalis pars thoracic (ICPT) muscles with normalized measured EMG signals (Arjmand et al. 2010); **b** computed passive, active and total forces of ICPT and LGPT for each side during forward flexion; **c** muscle wrapping for LGPT and ICPT at full-flexion with generated contact forces. Model parameters fitting the subject in measurements: sex = male, age = 52 years, BW = 68.4 kg and BH = 174.5 cm

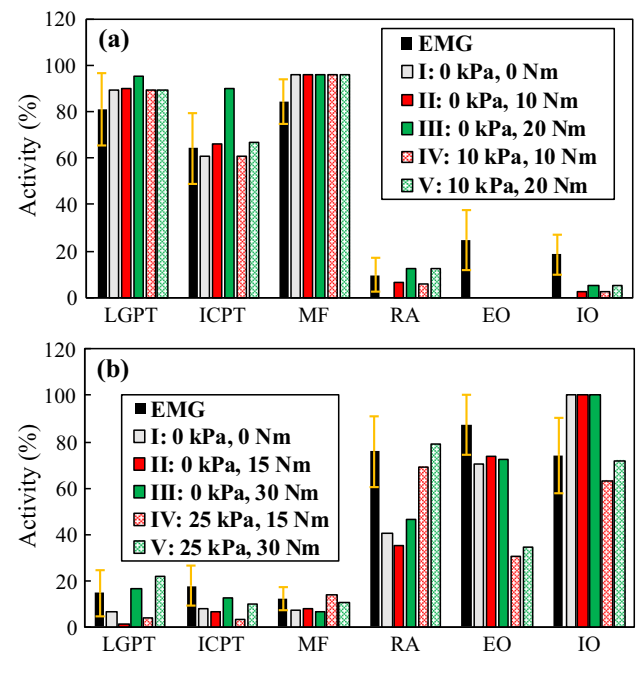
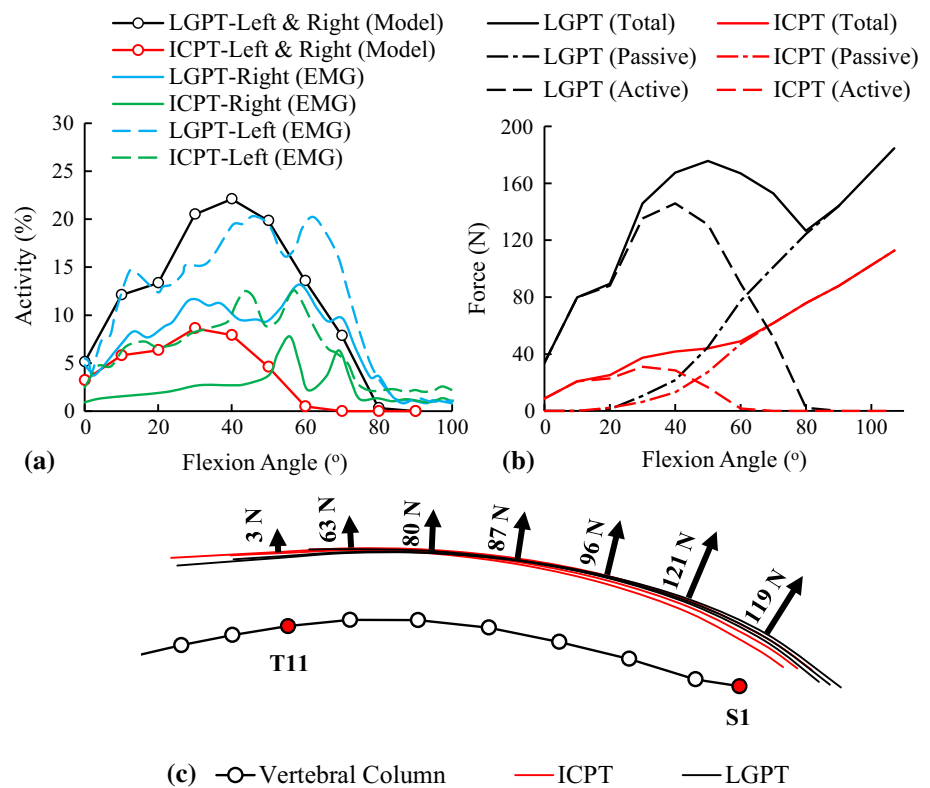


Fig. 7 Calculated muscle activities at MVE tasks **a** under 242Nm extension moment (average of 12 subjects) for different values of intra-abdominal pressure (IAP) (0 and 10 kPa) and antagonist moment (0, 10 and 20 Nm), Table 3, and **b** under 151 Nm flexion moment (average of 12 subjects) for different values of IAP (0 and 25 kPa) and antagonist moment (0, 15 and 30 Nm), Table 3, versus normalized EMG (Ouaaid et al. 2013). Model parameters fitting mean of subjects: sex = male, age = 25 years, BW = 72.98 kg and BH = 177.67 cm

Ng et al. 2002; Wilke et al. 2001) that are simulated here in this study on compression and shear forces at the L4–L5 level is investigated (Fig. 9) during forward flexion (task 7). Despite relatively small differences especially in BW (68–73 kg range) and BH (1.75–1.80 m range), relatively large differences are computed at larger flexion angles reaching peak differences of 21 % in compression and 30 % in shear.

4 Discussion

This study aimed to (1) markedly improve and personalize an existing trunk KD-FE musculoskeletal model and (2) develop a nonlinear regression equation to estimate IDP at the L4–L5 level as a function of its segmental compression force and sagittal rotation. The T11–T12 segment was added as a deformable body, the muscle architecture was updated with additional uni- and bi-articular muscles and a new model for the rectus sheath, and finally a novel automated scaling method was incorporated to personalize the entire model as subject sex, age, BW and BH change. This scaling framework modifies muscles geometry (i.e., length, area and lever arms), bony structures and passive joint properties. The personalized model was applied to a number of tasks and satisfactory agreement was found between predicted spinal IDPs and muscle activities with corresponding in vivo measurements (Arjmand et al. 2010; Ouaaid et al. 2013; Ng et al. 2002; Wilke et al. 2001).

Table 3 Considered IAPs and antagonistic coactivation moments as well as computed correlation coefficients between mean of estimated muscle activities (Fig. 7) and measured EMG (for 12 subjects [Ouaaid et al. 2013]) and applied shear forces (Eq. 4) in MVE tasks

	I	II	III	IV	V
Extension MVE task					
IAP (kPa)	0	0	0	10	10
Co-activation moment (Nm)	0	10	20	10	20
Correlation coefficient	0.99	0.98	0.96	0.98	0.97
Flexion MVE task					
IAP (kPa)	0	0	0	25	25
Co-activation moment (Nm)	0	15	30	15	30
Correlation coefficient	0.86	0.85	0.87	0.81	0.79
F_S^{T11} / F_S^{T12} (N)	641/486	688/NA ^a	657/NA	288/NA	356/NA

^a Not applied

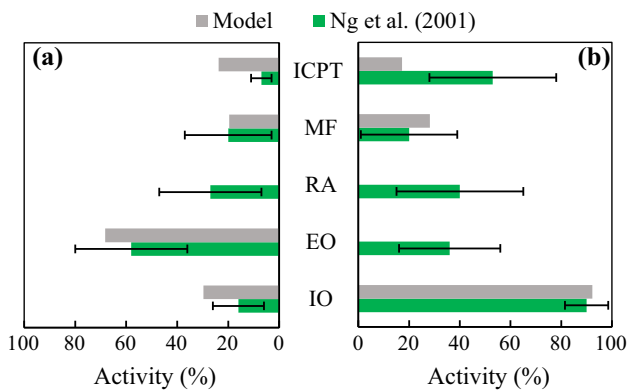


Fig. 8 Estimated muscle activities for the MVE task in torsion at upright standing versus measured EMG signals on **a** left and **b** right sides under 78.3Nm right axial torque along with 21.1Nm right lateral moment and 16.7Nm flexion moment (Ng et al. 2001). Fascicles with the maximum activity are reported for abdominal muscles. Model parameters used: sex = male, age = 30 years, BW = 73.00 kg and BH = 179.90 cm

4.1 Limitations and methodological issues

Since the model is driven by kinematics at different T11-S1 levels, the accuracy of measurements with motion capture camera systems and skin markers (due to the unavoidable inter skin-vertebrae and inter marker-skin movements) and subsequent partitioning of relative trunk-pelvis rotations among intervening T11-S1 levels remain of concern (Arjmand et al. 2010; Arjmand and Shirazi-Adl 2006a; El-Rich et al. 2004). To be consistent with our previous publications, we assumed maximum muscle stresses were 0.6 MPa despite using 1.0 MPa for demanding tasks. Stiffening the bending properties of the T11-T12 motion segment by 20% was assumed based on cadaver studies on the whole (Watkins 2005) and upper (Brasiliense et al. 2011) thoracic spine as well as the consideration of a floating rib at this level. While IAP was simulated with a normal load to the diaphragm, the detailed mechanism relating the generated pressure to activity in surrounding abdominal muscles was not considered

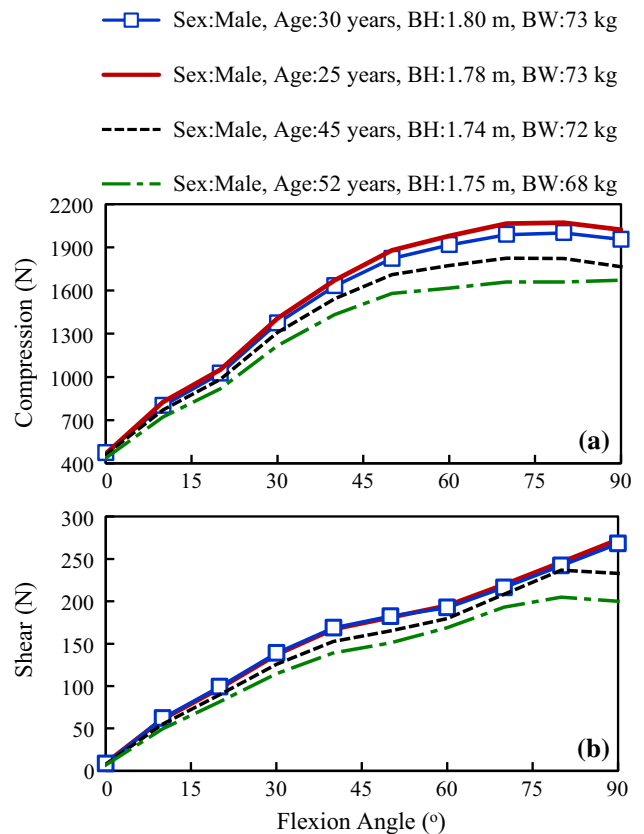


Fig. 9 Predicted local **a** compression and **b** shear forces at the L4-L5 disc for four different personal parameters used in this study

(Arjmand and Shirazi-Adl 2006b). Likely effects of inter-subject changes in initial spinal alignment and lordosis on results were neglected. Despite other imaging studies that report personalized moment arms and PCSAs (Chaffin et al. 1990; Jorgensen et al. 2001; Seo et al. 2003; Wood et al. 1996), we used here the data sets of Anderson et al. (2012) as they are comprehensive (100 females and males), not limited to the lumbar region and provide required regression equations accounting for sex, age, BH and BW; nevertheless, the

R^2 value is low for some of the reported regression equations. Utilizing the conventional beam theory as the scaling rule for passive joint properties, though plausible, involves some approximations. It is to be noted that a detailed FE model of the spine can address this scaling issue, nonetheless, the computational burden would be significant. In personalization of the model, disc heights were assumed to change proportionally to the BH. Although no study has yet investigated the correlation between BH and disc heights, experimental (Dimitriadis 2011) and modelling (Han et al. 2013) studies indirectly support our relation. Despite studies suggesting the effect of obesity (that can be interpreted as BW) (Lidar 2012; Urquhart 2014) and ageing (Videman et al. 2014) on disc heights, we did not adjust disc heights as BW and age vary. For BW, however and due to associated increase in compression on discs, disc heights reduce more in heavier subjects. In older subjects, ageing causes disc height loss (Videman et al. 2014) which should yield lower BH. Since we adjust disc heights with BH, the model accounts though indirectly for ageing effects on disc heights. Disc areas were assumed to vary proportional to the area of the rib cage since no study has quantified the effects of changes in BH and BW on disc areas. Furthermore, in the development of the IDP regression equations, although the compression was normalized to the disc total cross-sectional area but this latter was constant in corresponding analyses. The disc total area and individual nucleus and annulus areas could play a role. Finally future sensitivity analyses should shed light on the relative effect of changes in various individual parameters on model predictions.

4.2 Data analysis and interpretation

Comparing estimated IDPs of a musculoskeletal model with measurements is frequently used for validation (Bruno et al. 2015; Han et al. 2012; Mohammadi et al. 2015; Rajaei et al. 2015; Senteler et al. 2016). Although some studies (Dreischarf et al. 2013; Shirazi-Adl and Drouin 1988) provided a tool for such estimations, none explicitly incorporated the effect of intersegmental rotations, θ . Due to this simplification, those relations predict identical IDP for different values of θ (Fig. 4). For instance, under pure moment with no axial force, no IDP is hence estimated in direct contrast to measurements and predictions. Furthermore, the effect of θ on the IDP is found to depend on the compression force as it diminishes at larger axial forces (Fig. 4). Consequently, the intersegmental angle may be neglected with little loss of accuracy only at much larger compression forces. It is noteworthy that Shirazi-Adl and Drouin (1988) carried out simulations only on an L2–L3 motion segment. The FE model of (Shirazi-Adl 2006) has smaller disc area (1455 mm^2) but larger nucleus area (653 mm^2) in comparison with those of (Dreischarf et al. 2013) (1480 mm^2 and 624 mm^2).

Validation of model predictions were performed under numerous tasks for which either IDP was available or surface EMG were collected in earlier studies. In addition, the considerations of forward flexion postures on the one hand and MVE tasks on the other were deliberately made to investigate the relative accuracy of both passive and active components in the model under diverse sets of large loads and movements. Results overall demonstrated satisfactory agreements in estimated IDP and hence associated muscle forces and spinal compression, flexion relaxation under large forward flexion angles, maximum strength in different planes, wrapping of global extensor muscles and activities of antagonist muscles. Some differences can be due to technical EMG issues such as electrode placement and crosstalk (Soderberg and Knutson 2000; Türker 1993) or the model limitations.

Detailed finite element studies of spinal motion segments (Meijer et al. 2011; Natarajan and Andersson 1999; Niemeyer et al. 2012) and intervertebral discs (Cappetti et al. 2015) have demonstrated the substantial role of both disc height and disc area in joint passive responses. Hence, to scale passive properties, we employed here the conventional beam theory that also yields results in general agreement with those based on the parametric FE model studies of the L3–L4 motion segment (Natarajan and Andersson 1999). According to the proposed scaling scheme, variations in both disc height and disc area affect passive segmental stiffness. As an example, in comparison with the reference properties (Fig. 2), angular and linear (axial) segmental stiffness values of a male subject with $\text{BMI} = 25 \text{ kg/m}^2$ (the reference value) decreases by $\sim 5\%$ and 6% at shorter $\text{BH} = 160 \text{ cm}$ but increases by $\sim 8\%$ and 9% at taller $\text{BH} = 190 \text{ cm}$, respectively.

The developed scaling method employed regression equations reported in imaging studies (Anderson et al. 2012; Shi et al. 2014) and biomechanical principles to modify the musculature and passive joint properties in the subject-specific models. The regression equations can present mean values for a cohort of subjects with the same sex, age, BW and BH. With these regression equations employed in our scaling, a cohort-specific trunk model is therefore generated in this work. In this study and for meaningful comparisons, we personalized the model for each simulation in accordance with the reported personal parameters of in vivo studies. Finally as a preliminary study to investigate the effect of changes in age, sex, BW and BH on results, forward flexion of four different subjects were considered (Fig. 9). Despite relatively small changes in these parameters (i.e., 68–73 kg for BW, 1.74–1.80 cm for BH and 25–52 years for age), relatively large differences in spinal forces were estimated especially at larger trunk flexion angles. Maximum increases of 21% (410 N) in compression and 30% (72 N) in shear forces were found when the subject BH and BW increased only slightly from 1.75 m and 68 kg, respectively, to 1.80 m and 73 kg revealing the impor-

tance of the scaling. Utilizing a scaling algorithm along with the musculoskeletal modelling is therefore recommended in order to estimate more accurate results for individuals in a general population. Future studies will consider additional cases covering a comprehensive population with focus on the relative effect of greater changes in age, BW or BH when considered alone or combined.

In summary, we have presented a comprehensive personalized musculoskeletal trunk model and a novel regression equation relating IDP to normalized compression and sagittal rotation at the L4–L5 level. The model is an updated version of an existing one by adding a flexible level (T11–T12), extending muscle architecture and introducing the scaling concept. The described scaling framework modified muscles geometry and bony structures. Instead of personalizing solely geometric features, the scaling scheme altered passive joint properties as well for the first time. Moreover, by employing a detail FE model of the lumbar spine, we proposed a regression equation to estimate IDP at the L4–L5 disc as a function of the compression and the intersegmental angle. Predicted results were found in satisfactory agreement with reported IDP and surface EMG data under a number of tasks. Due to marked effects of personal parameters (e.g., stature, body weight) on results of musculoskeletal models, future model studies should incorporate comprehensive scaling techniques for more accurate estimation of spinal forces and muscle activity.

Acknowledgments This work was supported by the Institut de recherche Robert-Sauvé en santé et en sécurité du travail (IRSST-2014-0009) and the Natural Sciences and Engineering Research Council of Canada (RGPIN5596).

Compliance with ethical standards

Conflict of interest No conflict of interest to declare.

References

- Adams MA, Roughley PJ (2006) What is intervertebral disc degeneration, and what causes it? *Spine* 31:2151–2161
- Anderson DE, D'Agostino JM, Bruno AG, Manoharan RK, Bouxsein ML (2012) Regressions for estimating muscle parameters in the thoracic and lumbar trunk for use in musculoskeletal modeling. *J Biomech* 45:66–75
- Arjmand N, Gagnon D, Plamondon A, Shirazi-Adl A, Lariviere C (2009) Comparison of trunk muscle forces and spinal loads estimated by two biomechanical models. *Clin Biomech* 24:533–541
- Arjmand N, Gagnon D, Plamondon A, Shirazi-Adl A, Lariviere C (2010) A comparative study of two trunk biomechanical models under symmetric and asymmetric loadings. *J Biomech* 43:485–491
- Arjmand N, Plamondon A, Shirazi-Adl A, Lariviere C, Parnianpour M (2011) Predictive equations to estimate spinal loads in symmetric lifting tasks. *J Biomech* 44:84–91
- Arjmand N, Shirazi-Adl A (2006a) Model and in vivo studies on human trunk load partitioning and stability in isometric forward flexions. *J Biomech* 39:510–521
- Arjmand N, Shirazi-Adl A (2006b) Role of intra-abdominal pressure in the unloading and stabilization of the human spine during static lifting tasks. *Eur Spine J* 15:1265–1275
- Arjmand N, Shirazi-Adl A (2006c) Sensitivity of kinematics-based model predictions to optimization criteria in static lifting tasks. *Med Eng Phys* 28:504–514
- Arjmand N, Shirazi-Adl A, Bazrgari B (2006) Wrapping of trunk thoracic extensor muscles influences muscle forces and spinal loads in lifting tasks. *Clin Biomech* 21:668–675
- Arjmand N, Shirazi-Adl A, Parnianpour M (2007) Trunk biomechanical models based on equilibrium at a single-level violate equilibrium at other levels. *Eur Spine J* 16:701–709
- Arjmand N, Shirazi-Adl A, Parnianpour M (2008) Trunk biomechanics during maximum isometric axial torque exertions in upright standing. *Clin Biomech* 23:969–978
- Bazrgari B (2008) Biodynamic of the human spine. (Order No. NR47713, Ecole Polytechnique, Montreal (Canada)). ProQuest Dissertations and Theses, 310. Retrieved from <http://search.proquest.com/docview/304819192?accountid=40695>
- Bazrgari B, Shirazi-Adl A (2007) Spinal stability and role of passive stiffness in dynamic squat and stoop lifts. *Comput Method Biomech Biomed Eng* 10:351–360
- Bazrgari B, Shirazi-Adl A, Parnianpour M (2009) Transient analysis of trunk response in sudden release loading using kinematics-driven finite element model. *Clin Biomech* 24:341–347
- Bazrgari B, Shirazi-Adl A, Trottier M, Mathieu P (2008) Computation of trunk equilibrium and stability in free flexion-extension movements at different velocities. *J Biomech* 41:412–421
- Brasiliense LB, Lazaro BC, Reyes PM, Dogan S, Theodore N, Crawford NR (2011) Biomechanical contribution of the rib cage to thoracic stability. *Spine* 36:E1686–E1693
- Brown SH, Ward SR, Cook MS, Lieber RL (2011) Architectural analysis of human abdominal wall muscles: implications for mechanical function. *Spine* 36:355
- Bruno AG, Bouxsein ML, Anderson DE (2015) Development and validation of a musculoskeletal model of the fully articulated thoracolumbar spine and rib cage. *J Biomech Eng* 137:081003
- Cappetti N, Naddeo A, Naddeo F, Solitro G (2015) Finite elements/Taguchi method based procedure for the identification of the geometrical parameters significantly affecting the biomechanical behavior of a lumbar disc. *Comput Methods Biomech Biomed Eng* 1–8. doi:10.1080/10255842.2015.1128529
- Chaffin DB, Redfern MS, Erig M, Goldstein SA (1990) Lumbar muscle size and locations from CT scans of 96 women of age 40 to 63 years. *Clin Biomech* 5:9–16
- Cholewicki J, McGill SM (1996) Mechanical stability of the in vivo lumbar spine: implications for injury and chronic low back pain. *Clin Biomech* 11:1–15
- Christophy M, Senan NAF, Lotz JC, O'Reilly OM (2012) A musculoskeletal model for the lumbar spine. *Biomech Model Mechanobiol* 11:19–34
- da Costa BR, Vieira ER (2010) Risk factors for work-related musculoskeletal disorders: a systematic review of recent longitudinal studies. *Am J Ind Med* 53:285–323
- Damsgaard M, Rasmussen J, Christensen ST, Surma E, de Zee M (2006) Analysis of musculoskeletal systems in the AnyBody Modeling System. *Simul Model Pract Theory* 14:1100–1111
- Davis J, Kaufman KR, Lieber RL (2003) Correlation between active and passive isometric force and intramuscular pressure in the isolated rabbit tibialis anterior muscle. *J Biomech* 36:505–512
- De Leva P (1996) Adjustments to Zatsiorsky-Seluyanov's segment inertia parameters. *J Biomech* 29:1223–1230
- De Zee M, Hansen L, Wong C, Rasmussen J, Simonsen EB (2007) A generic detailed rigid-body lumbar spine model. *J Biomech* 40:1219–1227

- Delp SL et al (2007) OpenSim: open-source software to create and analyze dynamic simulations of movement. *IEEE Trans Biomed Eng* 54:1940–1950
- Delp SL, Suryanarayanan S, Murray WM, Uhlir J, Triolo RJ (2001) Architecture of the rectus abdominis, quadratus lumborum, and erector spinae. *J Biomech* 34:371–375
- Dimitriadis A et al (2011) Intervertebral disc changes after 1 h of running: a study on athletes. *J Int Med Res* 39:569–579
- Dreischarf M et al (2015) In vivo implant forces acting on a vertebral body replacement during upper body flexion. *J Biomech* 48:560–565
- Dreischarf M, Rohlmann A, Zhu R, Schmidt H, Zander T (2013) Is it possible to estimate the compressive force in the lumbar spine from intradiscal pressure measurements? A finite element evaluation. *Med Eng Phys* 35:1385–1390
- El-Rich M, Shirazi-Adl A (2005) Effect of load position on muscle forces, internal loads and stability of the human spine in upright postures. *Comput Method Biomech* 8:359–368
- El-Rich M, Shirazi-Adl A, Arjmand N (2004) Muscle activity, internal loads, and stability of the human spine in standing postures: combined model and in vivo studies. *Spine* 29:2633–2642
- El Ouaid Z, Arjmand N, Shirazi-Adl A, Parnianpour M (2009) A novel approach to evaluate abdominal coactivities for optimal spinal stability and compression force in lifting. *Comput Method Biomech* 12:735–745
- El Ouaid Z, Shirazi-Adl A, Plamondon A, Larivière C (2013) Trunk strength, muscle activity and spinal loads in maximum isometric flexion and extension exertions: A combined in vivo-computational study. *J Biomech* 46:2228–2235
- Ferguson S, Marras W (1997) A literature review of low back disorder surveillance measures and risk factors. *Clin Biomech* 12:211–226
- Gagnon D, Arjmand N, Plamondon A, Shirazi-Adl A, Larivière C (2011) An improved multi-joint EMG-assisted optimization approach to estimate joint and muscle forces in a musculoskeletal model of the lumbar spine. *J Biomech* 44:1521–1529
- Gardner-Morse MG, Stokes IA (2004) Structural behavior of human lumbar spinal motion segments. *J Biomech* 37:205–212
- Gayzik FS, Mao MY, Danelson KA, Slice DE, Stitzel JD (2008) Quantification of age-related shape change of the human rib cage through geometric morphometrics. *J Biomech* 41:1545–1554
- Gercek E, Hartmann F, Kuhn S, Degreif J, Rommens PM, Rudig L (2008) Dynamic angular three-dimensional measurement of multisegmental thoracolumbar motion in vivo. *Spine* 33:2326–2333
- Gerus P et al (2013) Subject-specific knee joint geometry improves predictions of medial tibiofemoral contact forces. *J Biomech* 46:2778–2786
- Ghezalbash F, Arjmand N, Shirazi-Adl A (2015) Effect of intervertebral translational flexibilities on estimations of trunk muscle forces, kinematics, loads, and stability. *Comput Method Biomech* 18:1760–1767
- Gilroy AM et al (2008) Atlas of anatomy. Thieme, Stuttgart
- Granata K, Marras W (1995) An EMG-assisted model of trunk loading during free-dynamic lifting. *J Biomech* 28:1309–1317
- Hajibozorgi M, Arjmand N (2016) Sagittal range of motion of the thoracic spine using inertial tracking device and effect of measurement errors on model predictions. *J Biomech* 49:913–918. doi:10.1016/j.jbiomech.2015.09.003
- Hajhosseinali M, Arjmand N, Shirazi-Adl A (2015) Effect of body weight on spinal loads in various activities: a personalized biomechanical modeling approach. *J Biomech* 48:276–282
- Han K-S, Rohlmann A, Zander T, Taylor WR (2013) Lumbar spinal loads vary with body height and weight. *Med Eng Phys* 35:969–977
- Han K-S, Zander T, Taylor WR, Rohlmann A (2012) An enhanced and validated generic thoraco-lumbar spine model for prediction of muscle forces. *Med Eng Phys* 34:709–716
- Heneweer H, Staes F, Aufdemkampe G, van Rijn M, Vanhees L (2011) Physical activity and low back pain: a systematic review of recent literature. *Eur Spine J* 20:826–845
- Jia B, Kim S, Nussbaum MA (2011) An EMG-based model to estimate lumbar muscle forces and spinal loads during complex, high-effort tasks: Development and application to residential construction using prefabricated walls. *Int J Ind Ergon* 41:437–446
- Jorgensen M, Marras W, Granata K, Wrand J (2001) MRI-derived moment-arms of the female and male spine loading muscles. *Clin Biomech* 16:182–193
- Keller TS, Colloca CJ, Harrison DE, Harrison DD, Janik TJ (2005) Influence of spine morphology on intervertebral disc loads and stresses in asymptomatic adults: implications for the ideal spine. *Spine J* 5:297–309
- Khurelbaatar T, Kim K, Kim YH (2015) A cervico-thoraco-lumbar multibody dynamic model for the estimation of joint loads and muscle forces. *J Biomech Eng* 137:111001
- Kiefer A, Shirazi-Adl A, Parnianpour M (1998) Synergy of the human spine in neutral postures. *Eur Spine J* 7:471–479
- Lidar Z et al (2012) Intervertebral disc height changes after weight reduction in morbidly obese patients and its effect on quality of life and radicular and low back pain. *Spine* 37:1947–1952
- Lund ME, Andersen MS, de Zee M, Rasmussen J (2015) Scaling of musculoskeletal models from static and dynamic trials. *Int Biomech* 2:1–11
- Martelli S, Kersh ME, Pandy MG (2015) Sensitivity of femoral strain calculations to anatomical scaling errors in musculoskeletal models of movement. *J Biomech* 48(13):3606–3615
- McGill SM (1996) A revised anatomical model of the abdominal musculature for torso flexion efforts. *J Biomech* 29:973–977
- Meijer GJ, Homminga J, Veldhuizen AG, Verkerke GJ (2011) Influence of interpersonal geometrical variation on spinal motion segment stiffness: implications for patient-specific modeling. *Spine* 36:E929–E935
- Meng X, Bruno AG, Cheng B, Wang W, Bouxsein ML, Anderson DE (2015) Incorporating six degree-of-freedom intervertebral joint stiffness in a lumbar spine musculoskeletal model—method and performance in flexed postures. *J Biomech Eng* 137:101008
- Mohammadi Y, Arjmand N, Shirazi-Adl A (2015) Comparison of trunk muscle forces, spinal loads and stability estimated by one stability- and three EMG-assisted optimization approaches. *Med Eng Phys* 37:792–800
- Nachemson A (1960) Lumbar intradiscal pressure: experimental studies on post-mortem material. *Acta Orthop* 31:1–104
- Natarajan RN, Andersson GB (1999) The influence of lumbar disc height and cross-sectional area on the mechanical response of the disc to physiologic loading. *Spine* 24:1873
- Ng JKF, Parnianpour M, Richardson CA, Kippers V (2001) Functional roles of abdominal and back muscles during isometric axial rotation of the trunk. *J Orthopaed Res* 19:463–471
- Ng JKF, Richardson CA, Parnianpour M, Kippers V (2002) EMG activity of trunk muscles and torque output during isometric axial rotation exertion: a comparison between back pain patients and matched controls. *J Orthop Res* 20:112–121
- Niemeyer F, Wilke H-J, Schmidt H (2012) Geometry strongly influences the response of numerical models of the lumbar spine—a probabilistic finite element analysis. *J Biomech* 45:1414–1423
- Oxland TR, Lin RM, Panjabi MM (1992) Three-dimensional mechanical properties of the thoracolumbar junction. *J Orthop Res* 10:573–580
- Paterson JK, Burn L (2012) Back pain: an international review. Springer Science & Business Media, Berlin
- Pearsall DJ (1994) Segmental inertial properties of the human trunk as determined from computed tomography and magnetic resonance imagery. Queen's University

- Phillips S, Mercer S, Bogduk N (2008) Anatomy and biomechanics of quadratus lumborum. *Proc Inst Mech Eng Part H: J Eng Med* 222:151–159
- Rajae MA, Arjmand N, Shirazi-Adl A, Plamondon A, Schmidt H (2015) Comparative evaluation of six quantitative lifting tools to estimate spine loads during static activities. *Appl Ergon* 48:22–32
- Rasmussen J, Zee Md, Damsgaard M, Christensen ST, Marek C, Siebertz K (2005) A general method for scaling musculo-skeletal models. In: International symposium on computer simulation in biomechanics
- Reeves NP, Cholewicki J (2003) Modeling the human lumbar spine for assessing spinal loads, stability, and risk of injury. *Crit Rev Biomed Eng* 31:73–139
- Rohlmann A, Dreischarf M, Zander T, Graichen F, Strube P, Schmidt H, Bergmann G (2013) Monitoring the load on a telemeterised vertebral body replacement for a period of up to 65 months. *Eur Spine J* 22:2575–2581
- Rozumalski A, Schwartz MH, Wervey R, Swanson A, Dykes DC, Novacheck T (2008) The in vivo three-dimensional motion of the human lumbar spine during gait. *Gait Posture* 28:378–384
- Sato K, Kikuchi S, Yonezawa T (1999) In vivo intradiscal pressure measurement in healthy individuals and in patients with ongoing back problems. *Spine* 24:2468
- Scheys L, Spaepen A, Suetens P, Jonkers I (2008) Calculated moment-arm and muscle-tendon lengths during gait differ substantially using MR based versus rescaled generic lower-limb musculoskeletal models. *Gait Posture* 28:640–648
- Schultz A, Andersson G, Ortengren R, Haderspeck K, Nachemson A (1982) Loads on the lumbar spine. Validation of a biomechanical analysis by measurements of intradiscal pressures and myoelectric signals. *J Bone Joint Surg* 64:713–720
- Senteler M, Weisse B, Rothenfluh DA, Snedeker JG (2016) Inter-vertebral reaction force prediction using an enhanced assembly of OpenSim models. *Comput Methods Biomech Biomed Eng* 19:538–548
- Seo A, Lee J-H, Kusaka Y (2003) Estimation of trunk muscle parameters for a biomechanical model by age, height and weight. *J Occup Health* 45:197–201
- Shahvarpour A, Shirazi-Adl A, Larivière C, Bazrgari B (2015a) Computation of trunk stability in forward perturbations-effects of preload, perturbation load, initial flexion and abdominal preactivation. *J Biomech* 48:716–720
- Shahvarpour A, Shirazi-Adl A, Larivière C, Bazrgari B (2015b) Trunk active response and spinal forces in sudden forward loading-analysis of the role of perturbation load and pre-perturbation conditions by a kinematics-driven model. *J Biomech* 48:44–52
- Shi X, Cao L, Reed MP, Rupp JD, Hoff CN, Hu J (2014) A statistical human rib cage geometry model accounting for variations by age, sex, stature and body mass index. *J Biomech* 47:2277–2285
- Shirazi-Adl A (1994a) Biomechanics of the lumbar spine in sagittal/lateral moments. *Spine* 19:2407–2414
- Shirazi-Adl A (1994b) Nonlinear stress analysis of the whole lumbar spine in torsion—mechanics of facet articulation. *J Biomech* 27:289–299
- Shirazi-Adl A (2006) Analysis of large compression loads on lumbar spine in flexion and in torsion using a novel wrapping element. *J Biomech* 39:267–275
- Shirazi-Adl A, Ahmed A, Shrivastava S (1986) A finite element study of a lumbar motion segment subjected to pure sagittal plane moments. *J Biomech* 19:331–350
- Shirazi-Adl A, Drouin G (1988) Nonlinear gross response analysis of a lumbar motion segment in combined sagittal loadings. *J Biomech Eng* 110:216–222
- Shirazi-Adl A, El-Rich M, Pop D, Parnianpour M (2005) Spinal muscle forces, internal loads and stability in standing under various postures and loads—application of kinematics-based algorithm. *Eur Spine J* 14:381–392
- Shirazi-Adl A, Parnianpour M (1993) Nonlinear response analysis of the human ligamentous lumbar spine in compression: on mechanisms affecting the postural stability. *Spine* 18:147–158
- Shirazi-Adl A, Sadouk S, Parnianpour M, Pop D, El-Rich M (2002) Muscle force evaluation and the role of posture in human lumbar spine under compression. *Eur Spine J* 11:519–526
- Soderberg GL, Knutson LM (2000) A guide for use and interpretation of kinesiological electromyographic data. *Phys Ther* 80:485–498
- Stokes IA, Gardner-Morse M (1999) Quantitative anatomy of the lumbar musculature. *J Biomech* 32:311–316
- Türker KS (1993) Electromyography: some methodological problems and issues. *Phys Ther* 73:698–710
- Urquhart DM et al (2014) Obesity is associated with reduced disc height in the lumbar spine but not at the lumbosacral junction. *Spine* 39:E962–E966
- Valente G, Pitto L, Stagni R, Taddei F (2015) Effect of lower-limb joint models on subject-specific musculoskeletal models and simulations of daily motor activities. *J Biomech* 48(16):4198–4205
- van Dieën JH, Cholewicki J, Radebold A (2003) Trunk muscle recruitment patterns in patients with low back pain enhance the stability of the lumbar spine. *Spine* 28:834–841
- Videman T, Battié MC, Gibbons LE, Gill K (2014) Aging changes in lumbar discs and vertebrae and their interaction: a 15-year follow-up study. *Spine J* 14:469–478
- Watkins R et al (2005) Stability provided by the sternum and rib cage in the thoracic spine. *Spine* 30:1283–1286
- Wilke H-J, Neef P, Hinz B, Seidel H, Claes L (2001) Intradiscal pressure together with anthropometric data—a data set for the validation of models. *Clin Biomech* 16:S111–S126
- Wilke HJ, Neef P, Caimi M, Hoogland T, Claes LE (1999) New in vivo measurements of pressures in the intervertebral disc in daily life. *Spine* 24:755–762
- Winter DA (2009) Biomechanics and motor control of human movement. Wiley, Toronto
- Wood S, Pearsall D, Ross R, Reid J (1996) Trunk muscle parameters determined from MRI for lean to obese males. *Clin Biomech* 11:139–144